# Mechanistic Studies of Ammonia Borane Dehydrogenation Catalyzed by Iron Pincer Complexes

Papri Bhattacharya, Jeanette A. Krause, and Hairong Guan*

Department of Chemistry, University of Cincinnati, P.O. Box 210172, Cincinnati, Ohio 45221-0172, United States

Ⓢ *Supporting Information*

ABSTRACT: A series of iron bis(phosphinite) pincer complexes with the formula of $[2,6-(^iPr_2PO)_2C_6H_3]Fe(PMe_2R)_2H$ (R = Me, **1**; R = Ph, **2**) or $[2,6-(^iPr_2PO)_2\text{-}4\text{-}(MeO)C_6H_2]Fe(PMe_2Ph)_2H$ (**3**) have been tested for catalytic dehydrogenation of ammonia borane (AB). At 60 °C, complexes **1**−**3** release 2.3−2.5 equiv of H_2 per AB in 24 h. Among the three iron catalysts, **3** exhibits the highest activity in terms of both the rate and the extent of H_2 release. The initial rate for the dehydrogenation of AB catalyzed by **3** is first order in **3** and zero order in AB. The kinetic isotope effect

(KIE) observed for doubly labeled AB ($k_{NH3BH3}/k_{ND3BD3} = 3.7$) is the product of individual KIEs ($k_{NH3BH3}/k_{ND3BH3} = 2.0$ and $k_{NH3BH3}/k_{NH3BD3} = 1.7$), suggesting that B−H and N−H bonds are simultaneously broken during the rate-determining step. NMR studies support that the catalytically active species is an AB-bound iron complex formed by displacing *trans* PMe_3 or PMe_2Ph (relative to the hydride) by AB. Loss of NH_3 from the AB-bound iron species as well as catalyst degradation contributes to the decreased rate of H_2 release at the late stage of the dehydrogenation reaction.
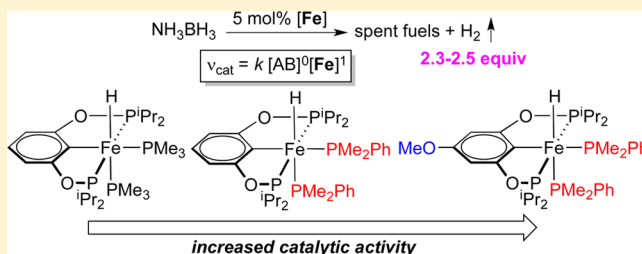
■ INTRODUCTION

Ammonia borane (AB = NH_3BH_3), a molecule first synthesized and characterized by Shore and Parry in 1955,[1] has been studied extensively in recent years, largely due to its potential to be utilized as a chemical hydrogen-storage material.[2] Although releasing H_2 from AB takes place thermally without a catalyst,[3] high temperatures and slow reaction rates are the main drawbacks that would impede the practical use of AB as a carrier for dihydrogen. In contrast, metal-catalyzed release of H_2 from AB could operate at a lower temperature and produce H_2 at a much faster rate. Additionally, the extent of H_2 released could be higher in a metal-catalyzed process, thereby taking advantage of the high gravimetric capacity of hydrogen in AB (19.6 wt %). Driven by these benefits, sufficient efforts have been made to develop catalytic systems for AB dehydrogenation.[2] Some of the most efficient catalysts include Heinekey and Goldberg's iridium POCOP-pincer complex (0.25−1 mol %, 1 equiv of H_2 per AB, RT, 3−36 min),[4] Fagnou's ruthenium phosphino-amine complexes (0.03−0.1 mol %, ~1 equiv of H_2 per AB, RT, 5−15 min),[5] Schneider's ruthenium PNP-pincer complex (0.01−0.1 mol %, 0.8−1 equiv of H_2 per AB, RT, 3−20 min),[6] and Kang's cationic Pd(II) complexes (3 mol %, 2 equiv of H_2 per AB, 25 °C, <1 min).[7] For catalytic systems with high extent of H_2 release, Manners' heterogeneous rhodium system (1.2 mol %, 45 °C, 48−84 h),[8] Baker's nickel NHC complexes (5 mol %, 60 °C, 4 h),[9] Williams' ruthenium bis(pyridyl)borate complex (5 mol %, 70 °C, 0.5 h),[10] and Jagirdar's $(\eta^6\text{-}C_6H_6)Cr(CO)_3$ (2 mol %, 0 °C, hυ, 1.5 h)[11] have been shown to release >2 equiv of H_2 per AB.

Developing iron-based catalytic systems would be even more desirable because iron is relatively inexpensive and the most abundant transition metal.[12] To date, only a handful of iron catalysts have been reported for the dehydrogenation of AB (Figure 1). Baker et al. have shown that $FeH(CH_2PMe_2)(PMe_3)_3$ (**A**), which is in an equilibrium with $Fe(PMe_3)_4$,[13] catalyzes the release of H_2 from AB at 20 °C.[9] The low thermal stability of this particular iron complex, however, results in significant decomposition and loss of catalytic activity over time. A more recent study by Baker, Gordon, and co-workers has focused on a series of iron complexes bearing both amido
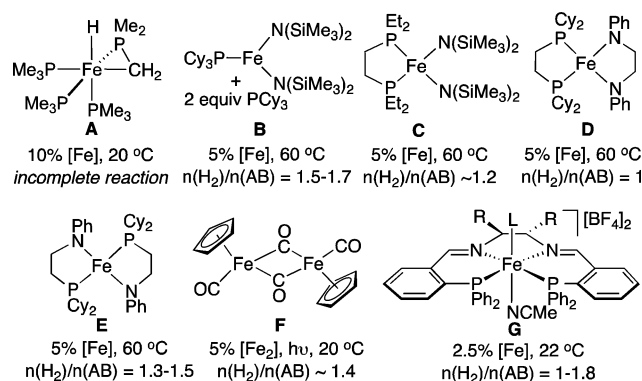

Figure 1. Iron-based catalysts for the dehydrogenation of AB and the extent of H_2 released in aprotic solvents.

and phosphine ligands (**B−E**).[14] These compounds are active at 60 °C and typically release 1−1.7 equiv of H$_2$ per AB; catalyst stability under the reaction conditions remains an issue, though. The Manners group has utilized [CpFe(CO)$_2$]$_2$ (**F**) to catalyze the dehydrogenation of AB[15] and its related amine boranes,[16] and CpFe(CO)$_2$I to catalyze the dehydrogenation of Me$_2$NHBH$_3$.[16] However, the catalysts need to be activated through photoirradiation. Sonnenberg and Morris have recently reported a highly efficient catalyst system involving iron complexes supported by a tetradentate bis(iminophosphine) ligand (**G**).[17] In the presence of large excess of KO^{t}Bu, these complexes have been shown to release H$_2$ at a rate up to 3.66 s^{-1} (H$_2$ per Fe). Interestingly, mechanistic investigation has suggested that the active species are not homogeneous molecular catalysts but zerovalent iron nanoparticles stabilized by the tetradentate ligand.

We have been interested in developing more robust iron catalysts for the activation of small molecules including AB. In particular, we have chosen pincer ligands[18] for the catalyst design because of their high tunability and, more importantly, the ability to minimize the degradation of iron complexes.[19] In our recent report,[20] we have demonstrated that iron bis(phosphinite) or POCOP-pincer complex **1** (Figure 2) is
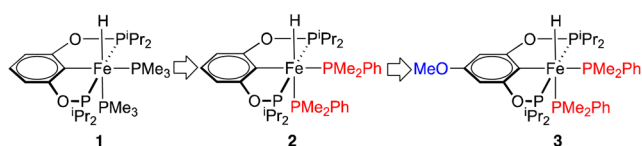
Figure 2. Iron POCOP-pincer complexes.

an effective catalyst for the hydrosilylation of aldehydes and ketones. Mechanistic studies have indicated that dissociation of the *trans*-PMe$_3$ (relative to the hydride) provides a vacant coordination site for substrate activation. We surmised that the coordinatively unsaturated intermediate might interact with AB as well to release H$_2$, and the rigidity of the pincer framework could make the catalyst long-lived. Because phosphine dissociation was thought to be the key to unlock the catalytic activity of the pincer complex, two structural modifications were made to expedite this process. In compound **2**, a more bulky ancillary ligand, PMe$_2$Ph, is used in place of PMe$_3$.[21] In the case of **3**, an electron-donating MeO group is also introduced at the *para* position to the *ipso* carbon for increased electron density at the iron center.

In this paper, we will show that complexes **1−3** are active catalysts for the dehydrogenation of AB, releasing more H$_2$ per AB than any of the iron-based catalytic systems reported to date.[22] Detailed NMR and kinetics studies including isotope effect measurements support the homogeneous nature of our catalytic system and the involvement of the pincer backbone in the catalytic reactions. Deactivation pathways for the iron catalysts at the late stage of the dehydrogenation reactions will also be discussed.

■ RESULTS

Synthesis and Structure of Iron Pincer Complexes. Following a similar procedure used for the synthesis of **1**,[20] iron POCOP-pincer complexes **2** and **3** were prepared from "Fe(PMe$_2$Ph)$_4$"[23] and an appropriate diphosphinite (eq 1). In this case, cyclometalation of the diphosphinite ligand is considerably slower, requiring as long as 48 h to complete
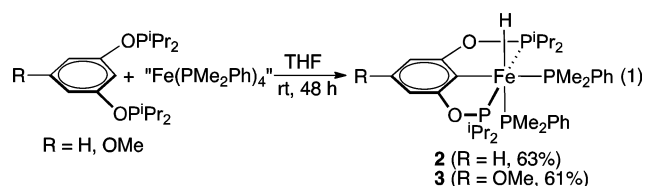
the reaction. By comparison, synthesis of **1** from 1,3-(^{i}Pr$_2$PO)$_2$C$_6$H$_4$ and Fe(PMe$_3$)$_4$ finishes within 3 h, probably because PMe$_3$ is less sterically bulky and more electron-donating, resulting in more facile oxidative addition of the C−H bond.

Compound **2** (in THF-d_8) displays a characteristic hydride resonance at −15.04 ppm as a triplet of doublet of doublets (tdd). On the basis of our previous study of related iron pincer complexes,[20] the J_{P-H} coupling constants of 76.8, 48.0, and 23.2 Hz are attributed to coupling with phosphorus nuclei from the pincer ligand, *cis*- and *trans*-PMe$_2$Ph, respectively. As expected, the ^{31}P{^{1}H} NMR spectrum of the same solution shows a doublet of doublets (dd) at 217.4 ppm and a pair of doublet of triplets (dt) at 23.7 and 14.6 ppm. The NMR data of **3** are similar to those of **2**; the hydride resonance is located at −15.32 ppm (tdd, J = 77.5, 48.1, and 24.9 Hz) and phosphorus resonances are found at 218.8 (dd), 23.9 (dt), and 15.0 (dt) ppm. The presence of the hydride ligand in **2** and **3** was further supported by IR spectroscopy, which exhibits a sharp band of medium intensity at 1890 (for **2**) or 1927 cm^{-1} (for **3**) as anticipated for the Fe−H stretch.

The structure of **3** was also established by X-ray crystallography. As illustrated in Figure 3, the hydride was
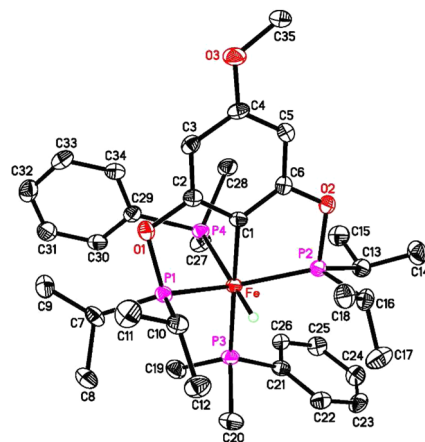
Figure 3. ORTEP drawing of [2,6-(^{i}Pr$_2$PO)$_2$-4-(MeO)C$_6$H$_2$]Fe(H)-(PMe$_2$Ph)$_2$ (**3**) at the 50% probability level. Selected bond lengths (Å) and angles (deg): Fe−H 1.21(4), Fe−C(1) 2.015(4), Fe−P(1) 2.1903(11), Fe−P(2) 2.1917(11), Fe−P(3) 2.2210(11), Fe−P(4) 2.2789(11), C(1)−Fe−P(1) 76.61(11), C(1)−Fe−P(2) 77.64(11), C(1)−Fe−P(4) 82.98(11), P(1)−Fe−P(4) 99.21(4), P(2)−Fe−P(4) 104.41(4), P(3)−Fe−P(4) 100.07(4), P(1)−Fe−P(3) 102.02(4), P(2)−Fe−P(3) 102.23(4), P(1)−Fe−P(2) 142.32(5).

located directly from the difference map and shown to be *cis* to the *ipso* carbon. The octahedral geometry around iron is significantly distorted and more so than that of **1**. To avoid the steric congestion incurred by the *trans*-PMe$_2$Ph, the pincer phosphorus atoms (P1 and P2) are shifted toward the hydride ligand (Figure 4) and displaced 0.5740(19) Å and 0.4510(20) Å out of the least-squares plane defined by the C1, O1, O2, and
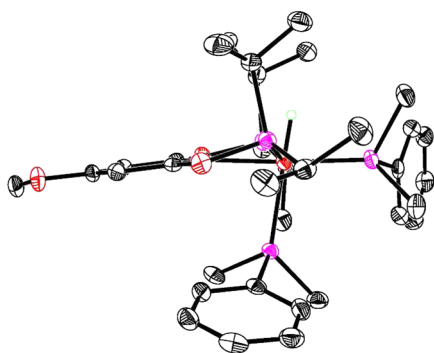
Figure 4. Side view of compound **3** (hydride shown in green).

Fe atoms.[24] The pincer aromatic ring (C1 through C6 plane) is tilted 8.41(5)° from the C1−O1−O2−Fe plane while leaning toward the *trans* PMe$_2$Ph. The Fe−P(4) distance [2.2789(11) Å] is longer than the Fe−P(3) distance [2.2210(11) Å], presumably due to a stronger *trans* influence of the hydride than the pincer aromatic ring. Compared to **1**, all the Fe−P bonds of **3** with the exception of the Fe−P3 bond are elongated by 0.02 Å, further suggesting that the iron center is more crowded.

Dehydrogenation of AB Catalyzed by 1−3. At room temperature, complex **1** shows no catalytic activity for the dehydrogenation of AB. At 60 °C, however, an immediate gas evolution was observed when a solution of **1** in THF was mixed with a solution of AB (20 equiv) in diglyme. The amount of H$_2$ was measured by displacing water from an inverted buret. After 24 h, 2.5 equiv of H$_2$ per AB was released (Figure 5). It should
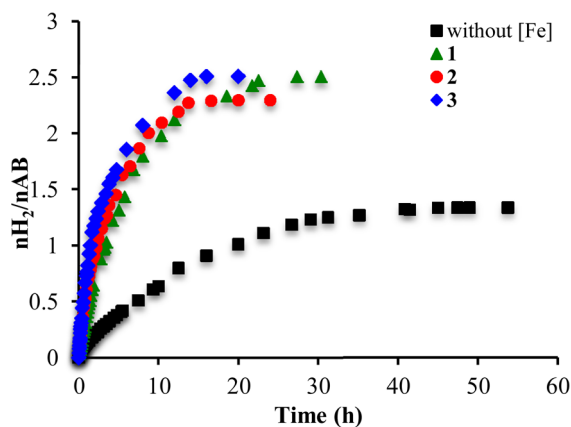

Figure 5. Amount of H$_2$ released from AB (1.0 M solution in 1:4 THF/diglyme) at 60 °C with or without an iron catalyst (5 mol %).

be mentioned that thermal decomposition of AB also takes place at 60 °C in THF/diglyme, but at a much slower rate. In addition, without a catalyst, the amount of H$_2$ released plateaued at ∼1.3 equiv of H$_2$ per AB. During the course of the dehydrogenation reaction catalyzed by **1**, the mixture gradually changed color from yellow to red, accompanied by a gray precipitate. The ^{11}B NMR spectrum of the soluble materials shows a doublet at 30.7 ppm and a broad singlet at 25.8 ppm, suggesting the formation of borazine and polyborazylene, respectively. Other observable boron resonances are a multiplet at −36.4 ppm for BH$_3$·PMe$_3$, and peaks within the range from −5 to −25 ppm that have been previously identified as cyclotriborazane (CTB)[3e,25] and *B*-

(cyclodiborazanyl)aminoborohydride (BCDB).[3e,26] The precipitate was characterized by IR, which shows a broad N−H band at 3213 cm^{-1} and almost no bands for the B−H stretch (Figure S2 in the Supporting Information [SI]).

Complex **2**, which differs from **1** only by the ancillary phosphine ligands, shows improved catalytic activity. When **2** and 20 equiv of AB were mixed in a similar fashion as the reaction with **1**, the color of the mixture changed from yellow to red immediately, indicative of a faster generation of the active species. The amount of H$_2$ produced in the beginning of the reaction was found to be higher than the reaction catalyzed by **1**. However, as time progressed, the solution became darkly colored, likely due to catalyst degradation. The decompostion of the catalyst was further substantiated by the fact that H$_2$ evolution ceased after approximately 12 h.

Complex **3** is a superior catalyst in terms of both rate and the extent of H$_2$ released (Figure 5). After 6 h of mixing, the ^{11}B NMR spectrum of the reaction (Figure S1 in the SI) indicates formation of borazine, polyborazylene, CTB, and BCDB. The multiplet observed at −37.7 ppm is assigned to BH$_3$·PMe$_2$Ph and integrated as 10 mol % of starting AB, suggesting that both PMe$_2$Ph ligands of **3** have been trapped by BH$_3$. Measuring H$_2$ evolution from this process gives 1.0 equiv, 2.0 equiv, and 2.5 equiv of H$_2$ per AB in 1.5, 7, and 16 h, respectively. Initiation of an active species from **3** appears to be as fast as **2**; an immediate color change from yellow to red was observed upon mixing **3** with AB. However, as illustrated by Figure 5, the amount of released H$_2$ still increases after 12 h, implying that the lifetime of the catalytically active species in this case is longer than that of **2**.

Although the reaction profiles in Figure 5 show no evidence for an induction period as commonly observed in heterogeneous catalysis,[27] the color change during the aforementioned dehydrogenation reactions, particularly in the case of **2**, cautioned us about the possibility of iron nanoparticles catalyzing the reaction. A commonly used method to distinguish between homogeneous and heterogeneous catalysis is the mercury test. However, as Morris et al. have pointed out,[28] Hg(0) may not form an amalgam with iron, therefore a negative mercury test is not sufficient to rule out a heterogeneous mechanism. Nevertheless, excess elemental mercury was added to the dehydrogenation of AB catalyzed by **1−3**, which resulted in no appreciable change in H$_2$ evolution (Figures S3−S5 in the SI). More definitive evidence supporting a homogeneous system for our iron POCOP-pincer catalysts is the reproducibility of the kinetics experiments that will be described in the next section.

While effective, all three iron complexes have a limited life span under catalytic conditions, either being converted to a catalytically less active species or being decomposed. For instance, when the reaction between **3** and 20 equiv of AB in THF/diglyme was complete (20 h at 60 °C), a second 20 equiv of AB was added, resulting in only 75% of AB being reacted after 24 h.

Kinetic Study. Reaction profiles for iron-catalyzed dehydrogenation of AB were also generated by monitoring the disappearance of AB by ^{11}B NMR spectroscopy (Figure 6). Treatment of the overall data shows a deviation from a first-order reaction; rather, two different rate regions are identified. At the beginning of the reaction, the decay of AB is fast and linear as a function of time. Later on, the dehydrogenation reaction becomes slower than what is expected for an exponential decay of AB. Since the kinetics changes over the
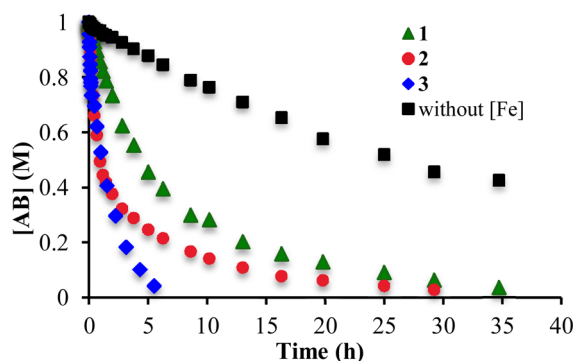
11155

dx.doi.org/10.1021/ja5058423 | *J. Am. Chem. Soc.* 2014, 136, 11153−11161

Figure 6. Disappearance of AB (1.0 M solution in 1:4 THF/diglyme) at 60 °C with or without an iron catalyst (5 mol %).
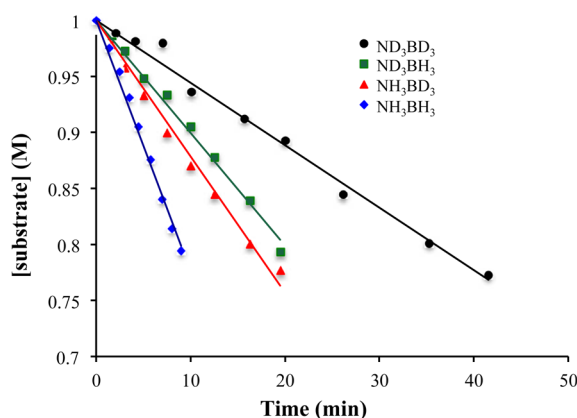

Figure 7. Disappearance of NH_3BH_3 and its isotopomers (1.0 M in 1:4 THF/diglyme) in the presence of 5 mol % of **3** at 60 °C. The concentrations of the substrates were determined from ^{11}B NMR.

course of the reaction and the background reaction comes to play as the reaction becomes slower, initial rates (20−25% conversion for AB) from the linear region of the plots were used for the kinetic study. The initial rates for the dehydrogenation of AB were measured as $(5.2 \pm 1.2) \times 10^{-5}$, $(2.3 \pm 0.5) \times 10^{-4}$, and $(3.5 \pm 0.3) \times 10^{-4}$ M/s for the reaction catalyzed by **1**−**3**, respectively. Initial rates determined from gas evolution measurements are similar except in the case of **1**, where the H_2 evolution rate is about twice that of the AB disappearance rate (Table S1 in the SI). Compared to the uncatalyzed thermal reaction, the rate for the dehydrogenation of AB catalyzed by **3** is about 50 times faster. Since **3** exhibits the highest catalytic activity among the three iron pincer complexes and it shows negligible decomposition at the early stage of the catalytic reaction, it was chosen as the catalyst for further mechanistic studies.

The dependence of dehydrogenation rate on substrate concentration was determined by measuring the initial rates ν_{obs} with variable $[AB]_0$ (0.75−2.0 M) but a fixed catalyst concentration of 0.050 M (Table S2 in the SI). Initial rates for the uncatalyzed thermal reaction (ν_{therm}) were also determined under similar reaction conditions (Table S3 in the SI). Catalytic rates ν_{cat} were then calculated by subtracting ν_{therm} from ν_{obs} for the same $[AB]_0$. Within the experimental errors, the value for ν_{obs} is constant, suggesting that the reaction has no dependence on the concentration of AB (Figure S6 in the SI). Similarly, to determine the reaction order for the catalyst, initial rates were measured by varying the catalyst loading (2.5−7.5 mol %) with a fixed initial AB concentration of 1.0 M. Plotting ln ν_{cat} against ln[Fe] gives a straight line with a slope of 1.04 ± 0.06 (Figure S7 in the SI). Thus, the dehydrogenation of AB in the presence of catalyst **3** is first order in **3** and zero order in AB (eq 2). The lack of dependence on the concentration of AB suggests that **3** may rapidly interact with AB and fully convert to an intermediate prior to the rate-determining step.

$$\nu_{cat} = k[AB]^0[3]^1 \qquad (2)$$

Despite the fact that the catalytic rate is independent of [AB], kinetic isotope effects (KIEs) should tell if N−H or B−H or both bonds are broken during the rate-determining step.[29] As illustrated in Figure 7 and Table S6 in the SI, deuteration of AB on either the nitrogen or the boron site results in a slower rate. The product of the individual KIEs [$(k_{NH3BH3}/k_{ND3BH3}) \times (k_{NH3BH3}/k_{NH3BD3}) = (2.0 \pm 0.3) \times (1.7 \pm 0.3) = (3.4 \pm 1.1)$] equals the KIE observed for the doubly labeled substrate [$(k_{NH3BH3}/k_{ND3BD3}) = (3.7 \pm 0.8)$], supporting a mechanism

where N−H and B−H bonds are broken simultaneously in the rate-determining step.

Stoichiometric and Catalytic Reactions of 3 with AB. To gain a better understanding of how **3** releases H_2 from AB, a reaction of **3** with one equivalent of AB in 1:4 THF-d_8/diglyme was studied by $^{31}P\{^1H\}$ and ^1H NMR spectroscopy. At room temperature, a new iron species **4** started to emerge in the $^{31}P\{^1H\}$ NMR spectrum as a doublet at 235.4 ppm (J_{P-P} = 13.0 Hz) and a triplet at 28.1 ppm (J_{P-P} = 13.0 Hz) with an integration ratio of 2:1. After 24 h, 15% of **3** was converted to **4** along with an equimolar amount of $BH_3 \cdot PMe_2Ph$, which was characterized as a quartet at 2.6 ppm (J_{P-B} = 56.8 Hz). At that point, the free diphosphinite ligand (~2% of the starting iron complex) was also observed as a singlet at 145.8 ppm. The same reaction performed at 60 °C for 10 min gave rise to a similar mixture plus a new iron species **5**, which was about 4% of total iron species. The phosphorus resonances of **5** are similar to those of **4**, featuring a doublet at 233.8 ppm (J_{P-P} = 29.2 Hz) and a triplet at 38.5 ppm (J_{P-P} = 29.2 Hz). The hydride region of the ^1H NMR spectrum displayed a broad resonance at −9.09 ppm and a multiplet at −14.42 ppm corresponding to **4**. The integration ratio of these two resonances was calculated to be 3:1. The hydride resonances of **5** were, however, too weak to be unambiguously located. Both $^{31}P\{^1H\}$ and ^1H NMR data suggest that **4** is produced as a result of one PMe$_2$Ph ligand of **3** (most likely the one *trans* to the hydride) being displaced by AB (Figure 8).[30] The broad resonance at −9.09 ppm can be assigned to the BH hydrogens.

A catalytic reaction of AB with **3** (5 mol % catalyst loading) in 1:4 THF-d_8/diglyme was also monitored by $^{31}P\{^1H\}$ and ^1H NMR spectroscopy. At 60 °C, **3** disappeared completely within 10 min, providing **4** as the major iron species (75% of total iron species) as well as $BH_3 \cdot PMe_2Ph$ (Figure 9). Of the three minor iron species, one is consistent with **5** as described above. The

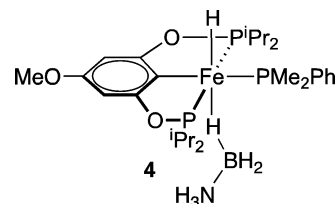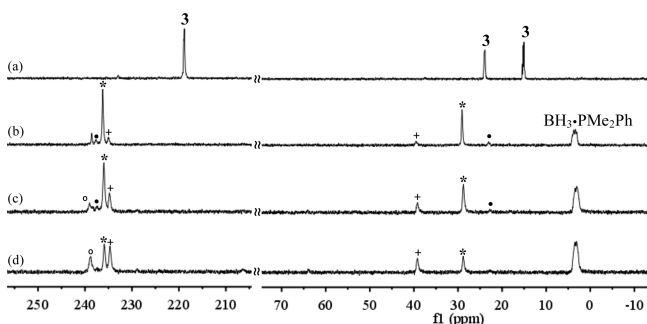**Figure 8.** Proposed structure of **4**.

Figure 9. $^{31}P\{^1H\}$ NMR spectra of (a) AB and **3** (5 mol % catalyst loading) mixed in 1:4 THF-d_8/diglyme at room temperature for 15 min, (b) heated at 60 °C for 10 min, (c) 60 °C for 1.5 h, and (d) 60 °C for 3 h (* for **4**, ● for **4'**, + for **5**, o for **6**).

resonance at 238.2 ppm (represented by the open circle in Figure 9) is a singlet, implying that both PMe$_2$Ph ligands have dissociated from iron. On the basis of our previous study of ligand substitution reaction for the related compound **1**, this resonance is attributed to a pincer complex (**6**) bearing two AB molecules. The resonances at 236.8 ppm (doublet, J_{P-P} = 26.0 Hz) and 22.1 ppm (triplet, J_{P-P} = 26.0 Hz) belong to one compound **4'**, which should contain only one PMe$_2$Ph ligand. This compound is likely to be the geometric isomer of **4** with PMe$_2$Ph bound *trans* rather than *cis* to the hydride. Compared to **4**, the more upfield shift of the PMe$_2$Ph resonance of **4'** is due to less shielding from the iron center induced by the strongly *trans*-influencing hydride ligand. As the reaction progressed, **4'** started to diminish, while the intensity of the resonance for **5** and **6** increased gradually. After 1.5 h, which was the time required to release 1 equiv of H$_2$ from AB, a small amount of other iron species became noticeable by $^{31}P\{^1H\}$ NMR. They are likely to be some iron complexes bearing partially dehydrogenated AB.

Compound **5** was thought to be a BH$_3$-coordinated complex resulting from **4** via the loss of NH$_3$. To generate **5** independently, **3** was treated with 2 equiv of BH$_3$·THF in 1:4 THF-d_8/diglyme. Immediately following the mixing at room temperature, 35% of **3** was reacted to yield **5** and its geometric isomer **5'** (Scheme 1). After 1.5 h, the conversion of **3** was increased slightly to 40% with substantially more **5'** being produced. Interestingly, replacing the mix-solvent with C$_6$D$_6$

Scheme 1. Room Temperature Reaction of 3 with BH$_3$·THF in 1:4 THF-d_8/Diglyme
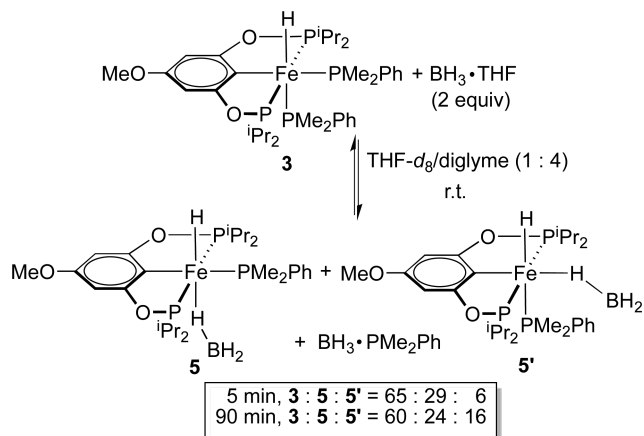
led to 60% conversion of **3** to **5** without the formation of **5'**.[31] The ratio between **3** and **5** stayed constant from 10 min to 24 h, suggesting that an equilibrium had been established. Evidently, the noncoordinating solvent benzene not only favors the dissociation of BH$_3$ from BH$_3$·THF, but also prevents the isomerization of **5** to **5'**.

Trapping of Aminoborane. Because more than 2 equiv of H$_2$ per AB were obtained from the catalytic reactions, it was anticipated that most, if not all, aminoborane (NH$_2$BH$_2$) was set free from the iron center. A metal-bound aminoborane would favor the formation of insoluble oligomers, leading to less H$_2$ production.[14,26] The presence of free aminoborane could be probed by using cyclohexene as a trapping agent, a method that was previously developed by Baker, Dixon, and co-workers.[26] Dehydrogenation of AB catalyzed by 5 mol % of **3** was therefore carried out in the presence of 20 equiv of cyclohexene with respect to AB. The trapping product H$_2$N—B(C$_6$H$_{11}$)$_2$ (47.8 ppm in ^{11}B NMR) was observed from the very beginning of the reaction. In addition to this boron species, a small amount of borazine and polyborazylene was also detected by ^{11}B NMR.

Cross-Coupling of NMe$_3$BH$_3$ and NH$_3$BEt$_3$. To indirectly determine whether H$_2$ is released from the same AB molecule or from intermolecular dehydrocoupling of two AB's, complex **3** was mixed with 20 equiv of NMe$_3$BH$_3$ and 20 equiv of NH$_3$BEt$_3$ in THF-d_8/diglyme. At 60 °C after 24 h, a small amount of H$_2$ was produced. According to ^{11}B NMR, only 29% of the combined starting materials reacted to generate BH$_3$·PMe$_2$Ph (5%) and some insoluble materials. This result suggests that intermolecular dehydrocoupling between NMe$_3$BH$_3$ and NH$_3$BEt$_3$ is possible, albeit at a rate that is substantially slower than the rate for the dehydrogenation of AB. These AB derivatives also trigger more rapid catalyst decomposition, leading to the free phosphinite ligand (>15% in 4 h at 60 °C) as confirmed by $^{31}P\{^1H\}$ NMR.

■ DISCUSSION

Reactivity Difference Among 1−3. The space-filling model of **1** and **3** (Figure 10) supports the notion that having
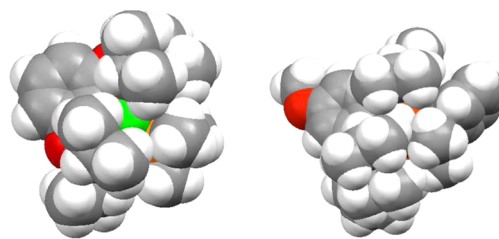

Figure 10. Space-filling model of **1** (left) and **3** (right). The hydride ligand is shown in green.

PMe$_2$Ph instead of PMe$_3$ as the ancillary ligand makes the iron center more crowded. As predicted, the rate for substituting CO for PMe$_2$Ph from **2** and **3** is much faster than the rate for substituting CO for PMe$_3$ from **1**.[32] Our previous work on complexes of this type shows that the kinetic substitution products are those with the *trans*-PMe$_3$ or PMe$_2$Ph being displaced by an incoming ligand.[20,32] These results are consistent with the *trans* effect order of H > Ar (aromatic ring). In comparison with **1**, the higher catalytic activity of **2** in the dehydrogenation of AB can be rationalized by a more rapid dissociation of the monophosphine. The reactivity of **3** is

11157

dx.doi.org/10.1021/ja5058423 | *J. Am. Chem. Soc.* 2014, 136, 11153−11161

further enhanced by the *p*-methoxy group, which provides more electron density to the iron center to facilitate ligand dissociation. The resulting coordinatively unsaturated intermediate, the presumed active species, is better stabilized by the more electron-donating PMe₃ or the methoxy group. The lifetime of the active catalyst formed from **1** or **3** is therefore longer than **2**, which is consistent with the observation that **1** and **3** outperform **2** for a higher amount of H₂ released (Figure 5).

Mechanism for the Early Stage of AB Dehydrogenation. Compared to Baker's iron systems,[9,14] incorporating a POCOP-pincer ligand in this work does show improved stability for iron catalysts, providing the opportunity to interpret the kinetic data at the molecular level. The diamagnetic nature of our iron complexes also allowed us to conveniently investigate the dehydrogenation reaction using NMR spectroscopy. As illustrated by Figure 9, the reaction of **3** with AB generates a mixture of iron species and the ratios of these species change over time, which inevitably complicates the kinetics for the overall dehydrogenation process. However, at the beginning of the reaction (<20 min, 20−25% conversion for AB), the dominant iron species is the AB-bound complex **4**. Therefore, it is reasonable to assume that **4** is responsible for the initial release of H₂. The lack of dependence of the initial rate on [AB] is due to a rapid conversion of **3** to **4** under the catalytic conditions. If the rate-determining step follows without the involvement of another AB molecule, the dehydrogenation rate would be first-order dependent on [Fe] as shown in eq 2. Williams and co-workers have also reported that the dehydrogenation of AB catalyzed by Shvo's catalyst is zero order in [AB] during the first two stages of the reaction.[33] They have attributed it to the dissociation of the starting diruthenium complex and the loss of H₂ from a hydroxycyclopentadienyl ruthenium hydride being the rate-determining step for the first and second stage of the dehydrogenation reaction. Schneider et al. have recently shown that dehydrogenation of ND₃BH₃ and ND₃BD₃ catalyzed by a 5-coordinate PNP-pincer ruthenium complex is zero order in the substrate for more than two half-lives.[34] Interestingly, dehydrogenation of the protio AB under otherwise the same reaction conditions exhibits first order in AB.

A mechanism that is consistent with our kinetic data including KIEs is outlined in Scheme 2. The proposed rate-determining step involves simultaneously breaking the N−H and B−H bonds of AB, which results in the protonation of the *ipso* carbon and the transfer of a hydride ligand from B to Fe. Such an activation pathway for AB or H₂ has been more commonly proposed in Noyori−Morris[35] or Shvo-type[36] bifunctional catalysts, where the metal center accepts a hydride and the neighboring heteroatom (nitrogen or oxygen) accepts a proton.[5,6,14,33] Direct participation of a carbon-based ligand in the activation of AB, H₂, or related molecules is less common, but not unprecedented. A computational study carried out by Yang and Hall[37] on Baker's Ni(NHC)₂ system[9] has revealed that dehydrogenation of AB starts with proton transfer from nitrogen to the carbene carbon. A more recent DFT study by Vanka et al. has further supported the feasibility of using a C−M bond as a motif for designing ligand−metal bifunctional catalysts.[38] Experimental observation of the dihydride species shown in Scheme 2 is, however, challenging. The analogous C−H bond activation to restore the pincer framework has been shown to be facile even at room temperature.[39] Alternative mechanisms without the protonation of the *ipso* carbon are less

Scheme 2. Proposed Catalytic Cycle for the Dehydrogenation of AB Catalyzed by 3
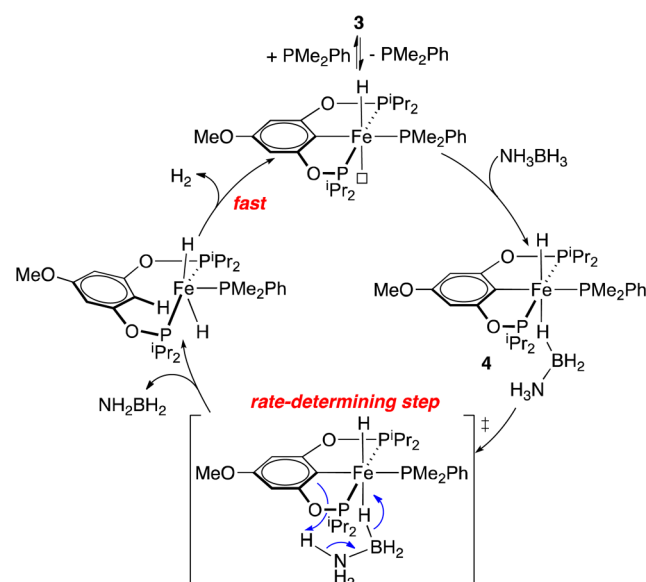
likely. To account for the observed rate law in eq 2 and the KIEs, one would have to propose a rapid loss of the second PMe₂Ph or the dissociation of a pincer arm,[40] followed by rate-limiting protonation of the hydride by the NH₃ moiety of AB. The NMR experiments described earlier show no evidence for the formation of a 5-coordinate intermediate. Dissociation of the second PMe₂Ph eventually takes place but at a rate too slow to explain the rapid catalysis at the beginning of the dehydrogenation process.

Catalyst Deactivation Pathways. Although the iron catalysts described herein have reasonable thermal stability, a number of pathways could potentially lead to a gradual loss of catalytic activity over time. In the case of **3** (Scheme 3), the

Scheme 3. Reaction Pathways for 4 under the Catalytic Conditions
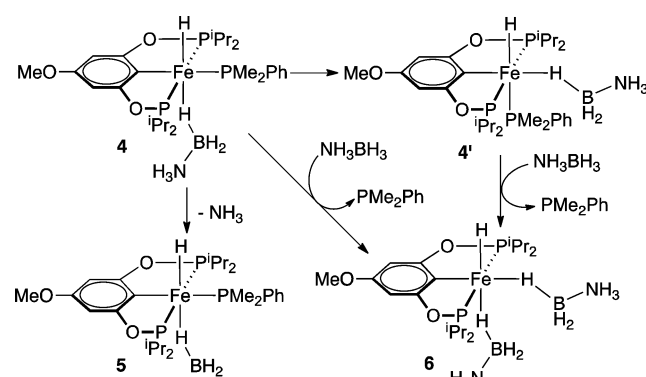
catalytically active species **4** undergoes a geometric isomerization to yield **4′**, placing the AB molecule *trans* to the *ipso* carbon. Under the catalytic conditions, a large excess of AB is available for further substitution of PMe₂Ph in **4′** to generate **6**, which contains two AB molecules. Alternatively, **4** can bypass **4′** and be converted to **6** directly. Perhaps **6** is capable of losing H₂ via a similar transition state as described for **4**. The formation of **4′** makes the protonation of the *ipso* carbon impossible, and prevents H₂ loss unless the NH₃ moiety of the

coordinated AB can protonate the hydride. A main catalyst deactivation pathway is the formation of **5** through the dissociation of NH_3 from **4**. As shown in Figure 9, its concentration is built up significantly after 3 h at 60 °C, thereby reducing the concentration of the catalytically active species.

Another catalyst deactivation pathway is the formation of the free diphosphinite ligand, which was observed from the stoichiometric reaction between **3** and AB. To our surprise, under the catalytic conditions, the free diphosphinite ligand was not detected by NMR. Decomplexation of the pincer ligand is somehow inhibited when AB is present in large excess. Nevertheless, the release of the diphosphinite ligand is expected toward the late stage of the dehydrogenation when the concentration of AB is substantially reduced. More pronounced catalyst degradation was observed when **3** was treated with NMe_3BH_3 and NH_3BEt_3. Upon interacting with the iron center, these more bulky substrates probably cause more structural perturbation to the complex, thereby facilitating aryl hydride reductive elimination to generate the free diphosphinite ligand.

CONCLUSIONS

In recent years, the interest in AB has been driven by its potential application as chemical hydrogen-storage materials. Although significant progress has been made in developing catalytic systems for the release of H_2 from AB, many challenges remain. In addition to identifying efficient and cost-effective methods to regenerate AB from spent fuels,[2f,41] there is also an important need for designing catalysts that are derived from earth-abundant metals and can release most of the available H_2 from AB.

Herein we have described an iron-based catalytic system releasing 2.3–2.5 equiv H_2 per AB, which, to the best of our knowledge, is the highest extent of H_2 release among all the iron systems known to date. Installing a POCOP-pincer ligand has been demonstrated as a key to stabilize the iron complexes and extend the lifetime of the iron catalysts for the release of H_2 over a long period of time. The relatively high stability of iron pincer complexes has also made mechanistic investigation possible. At the early stage of the dehydrogenation process, the catalytically active species is generated via a rapid dissociation of the phosphine ligand *trans* to the hydride, followed by the coordination of AB. The phosphine dissociation step can be promoted by a more bulky ligand and a more donating pincer ligand. The dehydrogenation reaction is first-order dependent on the iron catalyst and zero-order dependent on AB. The rate-determining step involves simultaneous transfer of H^- and H^+ from AB to the iron and pincer *ipso* carbon respectively, which has been supported by kinetic isotope effect measurements. As the dehydrogenation reaction proceeds, geometric isomerization of the AB-bound complex, further substitution of the phosphine by AB, dissociation of NH_3 from the AB-bound complex, and degradation of the iron complexes to the free diphosphinite ligand take place. At the very least the latter two processes are the culprits for the diminished catalytic activity toward the late stage of the dehydrogenation process. Our future efforts will be devoted to developing more robust and efficient iron pincer catalysts.

EXPERIMENTAL SECTION

General Comments. All the organometallic compounds were prepared and handled under an argon atmosphere using standard Schlenk and inert-atmosphere box techniques. Dry and oxygen-free solvents were collected from an Innovative Technology solvent purification system and used throughout all experiments. Methanol was degassed by bubbling argon through it for 15 min and then dried over molecular sieves. Tetrahydrofuran-d_8 (99.5% D, packed in sealed ampules) was purchased from Cambridge Isotope Laboratories, Inc. and used without further purification. Ammonia borane (AB), anhydrous diglyme, and NMe_3BH_3 were purchased from Sigma-Aldrich and used as received. ^1H, $^{13}C\{^1H\}$, and $^{31}P\{^1H\}$ NMR spectra were recorded on a Bruker Avance-400 MHz spectrometer. ^{11}B NMR spectra were recorded on a Bruker AMX 400 MHz wide-bore spectrometer. Chemical shift values in ^1H and ^{13}C NMR spectra were referenced internally to the residual solvent resonances. $^{31}P\{^1H\}$ and ^{11}B NMR spectra were referenced externally to 85% H_3PO_4 (0 ppm) and $BF_3 \cdot Et_2O$ (0 ppm), respectively. Infrared spectra were recorded on a Thermo Scientific Nicolet 6700 FT-IR spectrometer equipped with smart orbit diamond attenuated total reflectance (ATR) accessory. 1,3-$(^iPr_2PO)_2C_6H_4$,[42] 1,3-$(^iPr_2PO)_2$-5-OMe-C_6H_3,[43] and complex **1**[20] were prepared as described in the literature.

Preparation of "Fe(PMe$_2$Ph)$_4$". "Fe(PMe$_2$Ph)$_4$" was prepared according to a similar method that was reported for the synthesis of Fe(PMe$_3$)$_4$.[20,44] In a Schlenk flask under an argon atmosphere, Mg turnings (1.50 g, 61.7 mmol) were vigorously stirred for at least 24 h while being heated by a 130 °C oil bath. Once the flask was cooled down to room temperature, FeCl$_2$ (500 mg, 3.94 mmol), THF (15 mL), and PMe$_2$Ph (2.8 mL, 19.7 mmol) were added sequentially. The resulting mixture was stirred vigorously at room temperature for 2−3 h by which time the color of the mixture changed to yellowish brown. The volatiles were removed under the vacuum, and the remaining solid was treated with 30 mL of pentane. After filtration, removal of pentane from the filtrate under vacuum produced "Fe(PMe$_2$Ph)$_4$" as a sticky yellow solid (2.27g, 95% yield), which was used for the subsequent synthesis without further purification. NMR spectra of this material showed at least three different iron species, likely due to the activation of both aliphatic and aromatic C−H bonds. $^{31}P\{^1H\}$ NMR (162 MHz, C$_6$D$_6$, δ): −7.1 to −5.8 (br, 1P), 31.0−31.9 (br, 1P), 41.1−42.3 (br, 2P) (species 1); −37.6 (dt, J_{P-P} = 46.8 and 24.8 Hz, 1P), 29.3 (dd, J_{P-P} = 35.6 and 24.8 Hz, 2P), 39.5 (dt, J_{P-P} = 46.8 and 35.6 Hz, 1P) (species 2); −15.3 to −14.1 (m, 1P), 37.7 (m, 3P) (species 3).

Synthesis of [2,6-($^iPr_2PO$)$_2$-C$_6$H$_3$]Fe(H)(PMe$_2$Ph)$_2$ (2). 1,3-$(^iPr_2PO)_2C_6H_4$ (843 mg, 2.46 mmol) and "Fe(PMe$_2$Ph)$_4$" (1.5 g, 2.47 mmol) were mixed in 15 mL of THF at room temperature. The resulting mixture was stirred for 48 h, at which point the color of the solution changed from yellow to dark brown. The volatiles were removed under vacuum, and the yellowish residue was treated with a mixture of pentane and diethyl ether (20 mL each) and filtered through a pad of Celite. The volatiles were removed under vacuum to give a yellow oily residue, which was washed with cold methanol (5 mL × 3), and the remaining solid was dried under vacuum. The resulting slightly brownish solid was redissolved in diethyl ether and filtered through a pad of Celite. The filtrate was dried under vacuum to produce a yellow powder (1.05 g, 63% yield). The pure product should appear yellow in color. If needed, the steps from washing with cold methanol to filtration through Celite and drying under vacuum can be repeated to ensure the purity. ^1H NMR (400 MHz, THF-d_8, δ): −15.04 (tdd, J_{P-H} = 76.8, 48.0, and 23.2 Hz, Fe*H*, 1H), 0.97−1.05 (m, CHC*H$_3$*, 12H), 1.08−1.13 (m, CHC*H$_3$*, 12H), 1.17 (d, J_{P-H} = 3.4 Hz, P*Me$_2$*Ph, 6H), 1.64 (d, J_{P-H} = 3.8 Hz, P*Me$_2$*Ph, 6H), 2.14−2.18 (m, C*H*CH$_3$, 2H), 2.24−2.32 (m, C*H*CH$_3$, 2H), 6.28 (d, J_{P-H} = 7.4 Hz, Ar*H*, 2H), 6.60 (t, J_{P-H} = 7.4 Hz, Ar*H*, 1H), 7.20−7.26 (m, Ar*H*, 6H), 7.36 (t, J_{H-H} = 6.9 Hz, Ar*H*, 2H), 7.57 (t, J_{H-H} = 7.4 Hz, Ar*H*, 2H). $^{13}C\{^1H\}$ NMR (101 MHz, THF-d_8, δ): 18.2 (s, CHC*H$_3$*), 19.1 (s, CHC*H$_3$*), 19.9 (s, CHC*H$_3$*), 20.0 (s, CHC*H$_3$*), 21.2 (d, J_{P-C} = 20.6 Hz, P*Me$_2$*Ph), 27.6 (dd, J_{P-C} = 19.9 and 3.4 Hz, P*Me$_2$*Ph), 35.4 (s, CHC*H$_3$*), 35.4−35.8 (m, CHC*H$_3$*), 102.9−103.1 (m, Ar*C*), 123.2 (d, J_{P-C} = 3.4 Hz, Ar*C*), 127.9 (s, Ar*C*), 128.1 (d, J_{P-C} = 7.3 Hz, Ar*C*), 128.3 (d, J_{P-C} = 6.3 Hz, Ar*C*), 128.5 (s, Ar*C*), 131.0 (d, J_{P-C} = 9.5 Hz, Ar*C*), 131.2 (d, J_{P-C} = 8.0 Hz, Ar*C*), 148.8 (d, J_{P-C} = 24.8 Hz, Ar*C*), 148.8−149.1 (m, Ar*C*), 149.4 (d, J_{P-C} = 17.4 Hz, Ar*C*), 165.2 (td, J_{P-C} = 10.0 and 4.5 Hz, Ar*C*). $^{31}P\{^1H\}$ NMR (162 MHz, THF-d_8, δ): 14.6 (dt, J_{P-P} = 32.2 and 25.0 Hz, P*Me$_2$*Ph, 1P), 23.7 (dt, J_{P-P} = 32.2 and

13.2 Hz, PMe_2Ph, 1P), 217.4 (dd, J_{P-P} = 25.0 and 13.2 Hz, OP^iPr_2, 2P). IR (solid): ν_{Fe-H} =1890 cm^{-1}. Anal. Calcd for $C_{34}H_{54}FeO_2P_4$: C, 60.54; H, 8.07. Found: C, 60.40; H, 8.07.

Synthesis of {2,6-($^iPr_2PO$)$_2$-4-(OMe)C_6H_2}Fe(H)(PMe_2Ph)$_2$ (3). This compound was prepared in 61% yield by a procedure similar to that used for **2**. X-ray quality crystals of **3** were obtained from recrystallization of the iron complex in THF/diethyl ether at −30 °C. ^{1}H NMR (400 MHz, THF-d_8, δ): −15.32 (tdd, J_{P-H} = 77.5, 48.1, and 24.9 Hz, FeH, 1H), 0.95−1.04 (m, CHCH_3, 12H), 1.08−1.15 (m, CHCH_3, 12H), 1.18 (d, J_{P-H} = 5.3 Hz, PMe_2Ph, 6H), 1.62 (d, J_{P-H} = 5.5 Hz, PMe_2Ph, 6H), 2.09−2.21 (m, CHCH$_3$, 2H), 2.23−2.31 (m, CHCH$_3$, 2H), 3.65 (s, OCH_3, 3H), 6.02 (s, ArH, 2H), 7.21−7.28 (m, ArH, 6H), 7.38 (t, J_{H-H} = 7.4 Hz, ArH, 2H), 7.54 (t, J_{H-H} = 7.8 Hz, ArH, 2H). ^{13}C{^{1}H} NMR (101 MHz, THF-d_8, δ): 18.4 (s, CHCH$_3$), 19.3 (s, CHCH$_3$), 20.0 (s, CHCH$_3$), 20.2 (s, CHCH$_3$), 21.5 (d, J_{P-C} = 20.2 Hz, PMe_2Ph), 27.9 (dd, J_{P-C} = 20.2 and 4.0 Hz, PMe_2Ph), 35.7 (s, CHCH$_3$), 35.6−36.0 (m, CHCH$_3$), 55.2 (s, OCH$_3$), 91.0 (d, J_{P-C} = 1.4 Hz, ArC), 128.0 (s, ArC), 128.3 (d, J_{P-C} = 7.4 Hz, ArC), 128.4 (d, J_{P-C} = 6.2 Hz, ArC), 128.6 (s, ArC), 131.1 (d, J_{P-C} = 9.4 Hz, ArC), 131.3 (d, J_{P-C} = 8.1 Hz, ArC), 134.5−135.3 (m, ArC), 149.2 (d, J_{P-C} = 25.3 Hz, ArC), 149.7 (d, J_{P-C} = 16.2 Hz, ArC), 159.8 (d, J_{P-C} = 3.2 Hz, ArC), 164.6 (td, J_{P-C} = 10.0 and 3.6 Hz, ArC). ^{31}P{^{1}H} NMR (162 MHz, THF-d_8, δ): 15.0 (dt, J_{P-P} = 32.0 and 24.8 Hz, PMe_2Ph, 1P), 23.9 (dt, J_{P-P} = 32.0 and 13.4 Hz, PMe_2Ph, 1P), 218.8 (dd, J_{P-P} = 24.8 and 13.4 Hz, OP^iPr_2, 2P). IR (solid): ν_{Fe-H} = 1927 cm^{-1}. Anal. Calcd for $C_{35}H_{56}FeO_3P_4$: C, 59.67; H, 8.01. Found: C, 59.57; H, 8.19.

General Procedure for Measuring the Amount of H$_2$ Produced from Catalytic Dehydrogenation of AB. In a flame-dried 5 mL Schlenk tube, a 1.25 M diglyme solution of AB (0.6 mL, 0.75 mmol) was mixed with a 0.25 M THF solution of an iron catalyst (0.15 mL, 0.0375 mmol). The Schlenk tube was closed by a Teflon valve, and its side arm was attached to a Sigma-Aldrich gas measuring buret with a thin Tygon tubing. The entire system was purged with argon before the Teflon valve of the Schlenk tube was opened to equilibrate the system. The Schlenk tube was immersed in a 60 °C oil bath while keeping the reaction mixture stirring at a fixed rate of 300 rpm. The amount of H$_2$ evolved was measured at different time intervals.

General Procedure for Kinetic Study of Catalytic Dehydrogenation of AB. In a flame-dried J. Young NMR tube, a diglyme solution of AB (0.4 mL) was mixed with an appropriate amount of **3** dissolved in THF (0.1 mL). BF$_3$·Et$_2$O (sealed in a capillary tube) was added as an external standard. The NMR tube was then attached to a Schlenk line under an argon atmosphere. The solution was heated at 60 °C allowing H$_2$ to escape through the Schlenk line, which was connected to a bubbler (reactions in a sealed NMR tube without venting were much slower). ^{11}B NMR spectrum of the reaction mixture was recorded periodically to measure the change in [AB] over time. The rates for uncatalyzed reaction were measured similarly.

NMR Reaction of 3 with AB. In a flame-dried J. Young NMR tube, complex **3** (10 mg, 14.2 μmol) and AB (14.2 μmol for the stoichiometric reaction or 0.284 mmol for the catalytic reaction) were dissolved in THF-d_8 and diglyme (1:4). The progress of the reaction was monitored at room temperature by ^{1}H, ^{31}P{^{1}H}, and ^{11}B NMR. After 24 h, the NMR tube was connected to a Schlenk line filled with argon and heated at 60 °C. The reaction was further monitored at this temperature by NMR.

Procedure for the Trapping of Aminoborane. In a flame-dried J. Young NMR tube, **3** (17.6 mg, 25.0 μmol) and AB (15.4 mg, 0.5 mmol) were dissolved in the mixture of THF (0.1 mL) and diglyme (0.4 mL). Cyclohexene (1.01 mL, 10 mmol) was added to the NMR tube, which was then exposed to an argon atmosphere and heated at 60 °C. The progress of this reaction was monitored by ^{11}B NMR.

Synthesis of NH$_3$BEt$_3$. This compound was prepared according to a slightly modified procedure from the one described by Schneider and co-workers.[34] In a flame-dried Schlenk flask, a 0.50 M solution of NH$_3$ in 1,4-dioxane (50 mL, 25 mmol) was mixed with a 1.0 M solution of BEt$_3$ in hexane (20 mL, 20 mmol) at −78 °C. The mixture was gradually warmed to room temperature and stirred for 30 min. Volatiles were removed under vacuum, resulting in a clear oily material

(4.7 g, 95% yield). About 1.5 equiv of 1,4-dioxane per NH$_3$BEt$_3$ remained present despite prolonged drying, and therefore this material was used in further experiments. ^{1}H NMR (400 MHz, C_6D_6, δ): 0.25−0.35 (m, CH_2, 6H), 0.88−0.95 (m, CH_3, 9H), 1.83 (br, NH_3, 3H), 3.34 (s, CH_2 of 1,4-dioxane, 12 H). ^{13}C{^{1}H} NMR (101 MHz, C_6D_6, δ): 10.2 (s, CH$_3$), 14.8 (br, CH$_2$), 67.0 (s, CH$_2$ of 1,4-dioxane). ^{11}B NMR (128 MHz, C_6D_6, δ): −12.4 (s).

NMR Reaction of 3 with both NMe$_3$BH$_3$ and NH$_3$BEt$_3$. In a flame-dried J. Young NMR tube, complex **3** (12.3 mg, 17.5 μmol), NMe$_3$BH$_3$ (25.5 mg, 0.35 mmol), and NH$_3$BEt$_3$ (86.5 mg, 0.35 mmol) were mixed in THF-d_8 (70 μL) and diglyme (280 μL). BF$_3$·Et$_2$O (sealed in a capillary tube) was added as an external standard. The progress of the reaction was monitored by NMR at room temperature. After 24 h, the NMR tube was connected to a Schlenk line, exposed to an argon atmosphere, and heated at 60 °C. The reaction was further monitored at this temperature by NMR.

■ ASSOCIATED CONTENT

ⓢ Supporting Information
^{11}B NMR spectra of catalytic dehydrogenation of AB, IR spectrum of the insoluble materials obtained from AB dehydrogenation, complete details of the crystallographic study, kinetic data, and plots of these data. This material is available free of charge via the Internet at http://pubs.acs.org.

■ AUTHOR INFORMATION

Corresponding Author
hairong.guan@uc.edu

Notes
The authors declare no competing financial interest.

■ ACKNOWLEDGMENTS

■ REFERENCES

(1) Shore, S. G.; Parry, R. W. *J. Am. Chem. Soc.* **1955**, *77*, 6084−6085.

(2) (a) Stephens, F. H.; Pons, V.; Baker, R. T. *Dalton Trans.* **2007**, 2613−2626. (b) Marder, T. B. *Angew. Chem., Int. Ed.* **2007**, *46*, 8116−8118. (c) Peng, B.; Chen, J. *Energy Environ. Sci.* **2008**, *1*, 479−483. (d) Hamilton, C. W.; Baker, R. T.; Staubitz, A.; Manners, I. *Chem. Soc. Rev.* **2009**, *38*, 279−293. (e) Staubitz, A.; Robertson, A. P. M.; Manners, I. *Chem. Rev.* **2010**, *110*, 4079−4124. (f) Smythe, N. C.; Gordon, J. C. *Eur. J. Inorg. Chem.* **2010**, 509−521.

(3) Thermal decomposition of AB in the solid state, ionic liquids, or solutions: (a) Wolf, G.; Baumann, J.; Baitalow, F.; Hoffmann, F. P. *Thermochim. Acta* **2000**, *343*, 19−25. (b) Baitalow, F.; Baumann, J.; Wolf, G.; Jaenicke-Rößler, K.; Leitner, G. *Thermochim. Acta* **2002**, *391*, 159−168. (c) Stowe, A. C.; Shaw, W. J.; Linehan, J. C.; Schmid, B.; Autrey, T. *Phys. Chem. Chem. Phys.* **2007**, *9*, 1831−1836. (d) Bluhm, M. E.; Bradley, M. G.; Butterick, R., III; Kusari, U.; Sneddon, L. G. *J. Am. Chem. Soc.* **2006**, *128*, 7748−7749. (e) Shaw, W. J.; Linehan, J. C.; Szymczak, N. K.; Heldebrant, D. J.; Yonker, C.; Camaioni, D. M.; Baker, R. T.; Autrey, T. *Angew. Chem., Int. Ed.* **2008**, *47*, 7493−7496. (f) Al-Kukhun, A.; Hwang, H. T.; Varma, A. *Int. J. Hydrogen Energy* **2013**, *38*, 169−179.

(4) Denney, M. C.; Pons, V.; Hebden, T. J.; Heinekey, D. M.; Goldberg, K. I. *J. Am. Chem. Soc.* **2006**, *128*, 12048−12049.

(5) Blaquiere, N.; Diallo-Garcia, S.; Gorelsky, S. I.; Black, D. A.; Fagnou, K. *J. Am. Chem. Soc.* **2008**, *130*, 14034−14035.

(6) Käß, M.; Friedrich, A.; Drees, M.; Schneider, S. *Angew. Chem., Int. Ed.* **2009**, *48*, 905−907.

(7) Kim, S.-K.; Han, W.-S.; Kim, T.-J.; Kim, T.-Y.; Nam, S. W.; Mitoraj, M.; Piekoś, Ł.; Michalak, A.; Hwang, S.-J.; Kang, S. O. *J. Am. Chem. Soc.* **2010**, *132*, 9954−9955.

(8) Jaska, C. A.; Temple, K.; Lough, A. J.; Manners, I. *J. Am. Chem. Soc.* **2003**, *125*, 9424−9434.

(9) Keaton, R. J.; Blacquiere, J. M.; Baker, R. T. *J. Am. Chem. Soc.* **2007**, *129*, 1844−1845.

(10) Conley, B. L.; Guess, D.; Williams, T. J. *J. Am. Chem. Soc.* **2011**, *133*, 14212−14215.

(11) Bera, B.; Jagirdar, B. R. *Inorg. Chim. Acta* **2011**, *372*, 200−205.

(12) Plietker, B., Ed. *Iron Catalysis in Organic Chemistry: Reactions and Applications*; Wiley-VCH: Weinheim, Germany, 2008.

(13) (a) Rathke, J. W.; Muetterties, E. L. *J. Am. Chem. Soc.* **1975**, *97*, 3272−3273. (b) Karsch, H. H.; Klein, H.-F.; Schmidbaur, H. *Angew. Chem., Int. Ed. Engl.* **1975**, *14*, 637−638.

(14) Baker, R. T.; Gordon, J. C.; Hamilton, C. W.; Henson, N. J.; Lin, P.-H.; Maguire, S.; Murugesu, M.; Scott, B. L.; Smythe, N. C. *J. Am. Chem. Soc.* **2012**, *134*, 5598−5609.

(15) Vance, J. R.; Robertson, A. P. M.; Lee, K.; Manners, I. *Chem.—Eur. J.* **2011**, *17*, 4099−4103.

(16) Vance, J. R.; Schäfer, A.; Robertson, A. P. M.; Lee, K.; Turner, J.; Whittell, G. R.; Manners, I. *J. Am. Chem. Soc.* **2014**, *136*, 3048−3064.

(17) Sonnenberg, J. F.; Morris, R. H. *ACS Catal.* **2013**, *3*, 1092−1102.

(18) (a) Gossage, R. A.; van de Kuil, L. A.; van Koten, G. *Acc. Chem. Res.* **1998**, *31*, 423−431. (b) Albrecht, M.; van Koten, G. *Angew. Chem., Int. Ed.* **2001**, *40*, 3750−3781. (c) Singleton, J. T. *Tetrahedron* **2003**, *59*, 1837−1857. (d) van der Boom, M. E.; Milstein, D. *Chem. Rev.* **2003**, *103*, 1759−1792. (e) Liang, L.-C. *Coord. Chem. Rev.* **2006**, *250*, 1152−1177. (f) Nishiyama, H. *Chem. Soc. Rev.* **2007**, *36*, 1133−1141. (g) *The Chemistry of Pincer Compounds*; Morales-Morales, D., Jensen, C. M., Eds.; Elsevier: Amsterdam, 2007. (h) Choi, J.; MacArthur, A. H. R.; Brookhart, M.; Goldman, A. S. *Chem. Rev.* **2011**, *111*, 1761−1779. (i) Selander, N.; Szabó, K. J. *Chem. Rev.* **2011**, *111*, 2048−2076.

(19) For a review on iron pincer complexes, see: Bhattacharya, P.; Guan, H. *Comments Inorg. Chem.* **2011**, *32*, 88−112.

(20) Bhattacharya, P.; Krause, J. A.; Guan, H. *Organometallics* **2011**, *30*, 4720−4729.

(21) The Tolman cone angles for PMe₂Ph and PMe₃ are 122° and 118°, respectively. For details, see Tolman, C. A. *Chem. Rev.* **1977**, *77*, 313−348.

(22) In a protic solvent such as ⁱPrOH, iron complexes bearing a PNNP ligand (**G** in Figure 1) can release 2.5−2.9 equiv of H₂ per AB.[17] However, this process produces B(OⁱPr)₃ as the spent fuel, and the B−O bonds are too strong to allow the regeneration of AB. For this reason, studies of AB dehydrogenation have been focused on reactions carried out in aprotic solvents.

(23) See Experimental Section for details.

(24) The deviation from planarity for the C1−O1−O2−Fe plane was calculated to be 0.0027 Å.

(25) Gaines, D. F.; Schaeffer, R. *J. Am. Chem. Soc.* **1963**, *85*, 3592−3594.

(26) Pons, V.; Baker, R. T.; Szymczak, N. K.; Heldebrant, D. J.; Linehan, J. C.; Matus, M. H.; Grant, D. J.; Dixon, D. A. *Chem. Commun.* **2008**, 6597−6599.

(27) (a) Widegren, J. A.; Finke, R. G. *J. Mol. Catal. A: Chem.* **2003**, *198*, 317−341. (b) Crabtree, R. H. *Chem. Rev.* **2012**, *112*, 1536−1554.

(28) Mikhailine, A. A.; Maishan, M. I.; Lough, A. J.; Morris, R. H. *J. Am. Chem. Soc.* **2012**, *134*, 12266−12280.

(29) Even though ν_{cat} is independent of [AB], the k value for different isotopomers of AB could be different.

(30) Alternatively, AB may be σ-bonded to Fe via one of the B−H bonds. For reviews on σ-borane complexes, see: (a) Alcaraz, G.; Sabo-Etienne, S. *Coord. Chem. Rev.* **2008**, *252*, 2395−2409. (b) Lin, Z. *Struct. Bonding* **2008**, *130*, 123−148.

(31) We cannot rule out the possibility of THF molecule remaining coordinated to the boron in **5** and **5′**. The ¹¹B NMR of the reaction in Scheme 1 shows a broad singlet at 18.4 ppm in addition to a quartet of doublets at −37.5 ppm (J = 90.8 and 53.8 Hz) as expected for BH₃·PMe₂Ph. This result suggests that BH₃·THF undergoes rapid BH₃ exchange with **5** and **5′**.

(32) Upon exposure to 1 atm of CO, displacing the *trans*-PMe₂Ph from **2** and **3** by CO completes in 5 min, whereas the similar reaction with **1** requires 24 h to reach completion. For details, see: Bhattacharya, P. *Small Molecule Activation with Iron Pincer Complexes.* Ph.D. Thesis, University of Cincinnati: Cincinnati, 2014.

(33) (a) Conley, B. L.; Williams, T. J. *Chem. Commun.* **2010**, *46*, 4815−4817. (b) Lu, Z.; Conley, B. L.; Williams, T. J. *Organometallics* **2012**, *31*, 6705−6714.

(34) Marziale, A. N.; Friedrich, A.; Klopsch, I.; Drees, M.; Celinski, V. R.; Schmedt auf der Günne, J.; Schneider, S. *J. Am. Chem. Soc.* **2013**, *135*, 13342−13355.

(35) (a) Noyori, R.; Hashiguchi, S. *Acc. Chem. Res.* **1997**, *30*, 97−102. (b) Noyori, R.; Ohkuma, T. *Angew. Chem., Int. Ed.* **2001**, *40*, 40−73. (c) Clapham, S. E.; Hadzovic, A.; Morris, R. H. *Coord. Chem. Rev.* **2004**, *248*, 2201−2237. (d) Ikariya, T.; Blacker, A. J. *Acc. Chem. Res.* **2007**, *40*, 1300−1308. (e) Morris, R. H. *Chem. Soc. Rev.* **2009**, *38*, 2282−2291.

(36) Conley, B. L.; Pennington-Boggio, M. K.; Boz, E.; Williams, T. J. *Chem. Rev.* **2010**, *110*, 2294−2312.

(37) Yang, X.; Hall, M. B. *J. Am. Chem. Soc.* **2008**, *130*, 1798−1799.

(38) Ghatak, K.; Mane, M.; Vanka, K. *ACS Catal.* **2013**, *3*, 920−927.

(39) Xu, G.; Sun, H.; Li, X. *Organometallics* **2009**, *28*, 6090−6095.

(40) The mechanism involving the dissociation of the pincer arm cannot be exclusively ruled out here. However, such a mechanism is disfavored based on our mechanistic studies on the geometric isomerization of related 18-electron iron POCOP-pincer complexes, which argue against the dissociation of the pincer arm.[32]

(41) Sutton, A. D.; Burrell, A. K.; Dixon, D. A.; Garner, E. B., III; Gordon, J. C.; Nakagawa, T.; Ott, K. C.; Robinson, J. P.; Vasiliu, M. *Science* **2011**, *331*, 1426−1429.

(42) Pandarus, V.; Zargarian, D. *Organometallics* **2007**, *26*, 4321−4334.

(43) Vabre, B.; Spasyuk, D. M.; Zargarian, D. *Organometallics* **2012**, *31*, 8561−8570.

(44) Karsch, H. H. *Chem. Ber.* **1977**, *110*, 2699−2711.